SUPERCONDUCTIVITY

Correlating the charge-transfer gap to the maximum transition temperature in $Bi_2Sr_2Ca_{n-1}Cu_nO_{2n+4+\delta}$

Zechao Wang[1,2]†, Changwei Zou[3]†, Chengtian Lin[4], Xiangyu Luo[5], Hongtao Yan[5], Chaohui Yin[5], Yong Xu[3,6,7], Xingjiang Zhou[5], Yayu Wang[3,6]*, Jing Zhu[1,2]*

As the number of CuO_2 layers, n, in each unit cell of a cuprate family increases, the maximum transition temperature ($T_{c,max}$) exhibits a universal bell-shaped curve with a peak at $n = 3$. The microscopic mechanism of this trend remains elusive. In this study, we used advanced electron microscopy to image the atomic structure of cuprates in the $Bi_2Sr_2Ca_{n-1}Cu_nO_{2n+4+\delta}$ family with $1 \le n \le 9$; the evolution of the charge-transfer gap size (Δ) with n can be measured simultaneously. We determined that the n dependence of Δ follows an inverted bell-shaped curve with the minimum Δ value at $n = 3$. The correlation between Δ, n, and $T_{c,max}$ may clarify the origin of superconductivity in cuprates.

Identifying universal trends of the superconducting transition temperature (T_c) and its correlations to other physical parameters may provide crucial clues for elucidating the origin of superconductivity (*1*). For example, the isotope effect $T_c \propto 1/\sqrt{M}$, where M is the isotopic mass, has inspired the phonon-mediated pairing picture in establishing the microscopic theory of conventional superconductivity in metals and alloys (*2*, *3*). Since the discovery of high-T_c superconductivity in copper oxide materials (referred to as cuprates), there have been considerable efforts in understanding what controls T_c. There are two well-established trends about T_c in cuprates: One is the dome-shaped doping dependence of T_c for a specific cuprate compound, where the maximum T_c ($T_{c,max}$) is located at hole concentration $p \sim 0.16$ (*1*). The other is the variation of $T_{c,max}$ with the number of CuO_2 planes (n) per unit cell in a homologous series, which reaches the highest when $n = 3$ (*4*). Understanding the physical origin behind these empirical rules could lead to the eventual solution for the pairing-mechanism problem in cuprates (*1*, *4*).

Whereas the second trend remains universal for many cuprate families (Fig. 1A), the first is apparently violated in the trilayer cuprate $Bi_2Sr_2Ca_2Cu_3O_{10+\delta}$ (Bi-2223), which has the highest $T_{c,max}$ of ~115 K in the $Bi_2Sr_2Ca_{n-1}Cu_nO_{2n+4+\delta}$ family (Bi-family) compounds. Recent scanning tunneling microscopy (STM) studies (*5*) have shown that the superconducting gap of Bi-2223 decreases monotonously with p in the overdoped regime. Unexpectedly, the T_c in this doping range exhibits a plateau rather than a continuous drop, most likely owing to the existence of two types of inequivalent CuO_2 planes (*6*, *7*). By contrast, the Bi-2223 system provides an ideal platform for investigating the evolution of $T_{c,max}$ with n and the physical parameters that control $T_{c,max}$. A promising starting point is the Mott-insulating "parent" state ($p \sim 0$) of cuprates, where the electronic structure can be described by a single parameter referred to as the charge-transfer gap (CTG) Δ, the size of which varies from 1 to 3 eV (*8*). A previous STM work (*9*) in $Bi_2Sr_2Ca_{n-1}Cu_nO_{2n+4+\delta}$ and $Ca_{n+1}Cu_nO_{n+2}Cl_2$ with $n = 1$ and 2 suggests that $T_{c,max}$ is anticorrelated with the Δ, together with theoretical calculations (*10*–*12*). However, a measurement covering the whole homologous cuprate series has not yet been achieved because of two main obstacles. First, it is difficult to synthesize high-quality single crystals for $n \ge 4$ in any cuprate family, and it is even more difficult to reach the $p \sim 0$ limit. Second, most of the spectral information about cuprates cannot distinguish the distinct CuO_2 planes for $n \ge 3$.

The development of advanced electron microscopy enables one to achieve through-depth (defined in this paper as along the crystallographic c axis) imaging and carry out high-spatial (subangstrom)–resolution electron energy–loss spectrometry (EELS) experiments. Thus, it allows a local probe of the intrinsic structural and electronic properties in confined unit cells (*13*). Here, we used scanning transmission electron microscopy (STEM) and EELS techniques to directly image the layer-by-layer lattice configuration and electronic structure of the Bi-family cuprates, covering an unprecedented layer structure range with $1 \le n \le 9$.

Imaging the atomic structure of the Bi-family compounds with $1 \le n \le 9$.

The evolution of $T_{c,max}$ with n for the Bi-family cuprates is indicated with a bold orange line in Fig. 1A, which displays the universal bell-shaped trend (*14*–*19*). Owing to the high spatial resolution of the STEM technique, the layered atomic structure can be clearly visualized, as shown in Fig. 1B for an optimally doped Bi-2223 sample. Each Cu atom in the inner CuO_2 plane (IP) forms an in-plane CuO_4 plaquette, whereas in the outer CuO_2 planes (OP), the configuration is a CuO_5 pyramid with one apical oxygen (Fig. 1B, right). Some previous studies (*20*, *21*) have suggested that the different environments of IP and OP may have a profound influence on their superconducting properties, but their layer-resolved electronic properties remain to be unveiled.

Figure 1, C to K, displays a series of high-quality cross-sectional STEM images, in which $Bi_2Sr_2Ca_{n-1}Cu_nO_{2n+4+\delta}$ with $1 \le n \le 9$ are all identified. We obtained the data for $n \ge 3$ by carefully searching within a dozen Bi-2223 samples, which include very scarce regions that have four or more CuO_2 planes per unit cell. The details about the search and discovery of the $n > 3$ phases are shown in fig. S5. Because of the quasi-two-dimensional nature of Bi-family cuprates, it has been shown recently that all the essential electronic properties are contained within a unit cell, BiO/SrO charge reservoir layers plus the CuO_2 layers (*22*). The methodology used here opens a gate for studying multilayer cuprates.

Measuring the charge-transfer gap of the Bi-family compounds.

The electronic band structure of cuprates is well characterized by the in-plane Cu $3d_{x^2-y^2}$ and doped O $2p_x/2p_y$ orbitals (*23*). Within the Zaanen-Sawatzky-Allen scheme (*24*), the undoped cuprate is a charge-transfer–type Mott insulator, in which the lowest-energy excitation is from the O charge-transfer band (CTB) to the unoccupied upper Hubbard band (UHB) of the Cu sites, which is schematically illustrated in Fig. 2A. Figure 2B shows the STM spectra in three insulating Bi-family cuprates with $n = 1$, 2, and 3, in which the Δ value between the edges of CTB and UHB can be clearly extracted. The results here expand on those of previous studies (*9*) to $n = 3$ and reveal the same trend of a monotonic decrease of Δ from 1.5 eV in Bi-2201 to 1.0 eV in Bi-2212 and 0.7 eV in Bi-2223.

Upon hole doping, an additional feature emerges from the CTB that is known as the Zhang-Rice singlet (ZRS) band (Fig. 2C). This feature can be attributed to the hybridized state of a doped hole involving one Cu-3d and the four nearest O-2p orbitals (*25*). In this circumstance, the main features in the STM spectra are the spectral weight transfer from high energy to low energy and the gradual formation of the pseudogap (*26*); the Δ value becomes less well defined. Nevertheless, the energy difference between the centers of the ZRS

[1]National Center for Electron Microscopy in Beijing, School of Materials Science and Engineering, Key Laboratory of Advanced Materials (MOE), The State Key Laboratory of New Ceramics and Fine Processing, Tsinghua University, Beijing, P.R. China. [2]Ji Hua Laboratory, Foshan, Guangdong, P.R. China. [3]State Key Laboratory of Low-Dimensional Quantum Physics and Department of Physics, Tsinghua University, Beijing, P.R. China. [4]Max Planck Institute for Solid State Research, Stuttgart, Germany. [5]Beijing National Laboratory for Condensed Matter Physics, Institute of Physics, Chinese Academy of Sciences, Beijing, P.R. China. [6]New Cornerstone Science Laboratory, Frontier Science Center for Quantum Information, Beijing, P.R. China. [7]RIKEN Center for Emergent Matter Science (CEMS), Wako, Japan.
†These authors contributed equally to this work.
*Corresponding author. Email: jzhu@mail.tsinghua.edu.cn (J.Z.); yayuwang@mail.tsinghua.edu.cn. (Y.W.)

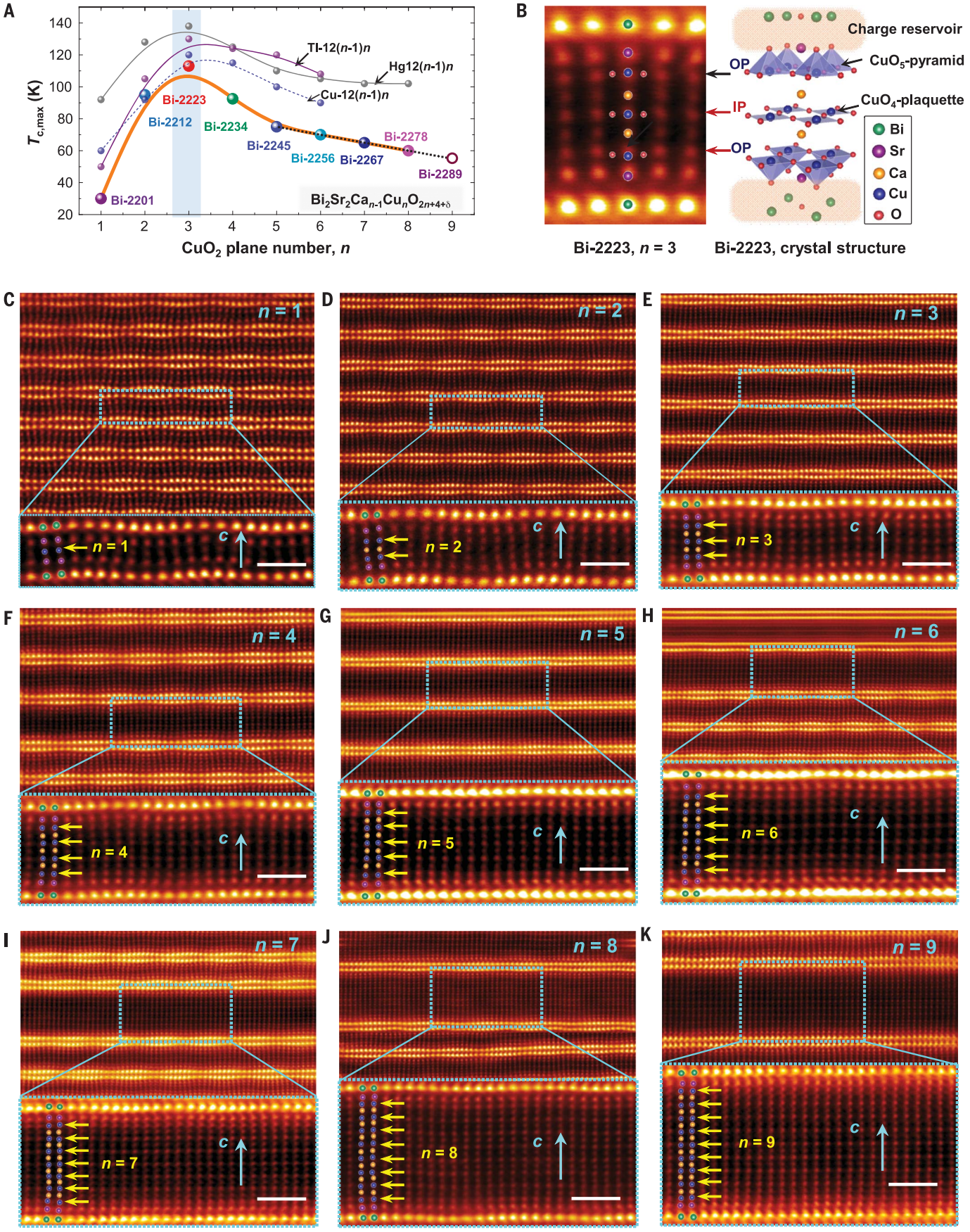

Figure 1

Fig. 1. The $T_{c,max}$ and atomically resolved crystal structure of $Bi_2Sr_2Ca_{n-1}Cu_nO_{2n+4+\delta}$ cuprates with $1 \le n \le 9$. (**A**) Relationship between $T_{c,max}$ and n for the homologous series of n-layered cuprates (*14*–*19*) including Tl-12(n-1)n, Hg-12(n-1)n, Cu-12(n-1)n, and Bi-22(n-1)n. The bold orange line indicates the $T_{c,max}$ as a function of n in the Bi-family. The n = 9 phase has never been discovered, so the $T_{c,max}$ value was obtained with linear extrapolation (as indicated with the black dotted line) and represented by a hollow circle. (**B**) A zoomed-in area of the n = 3 sample (Bi-2223) with the schematic crystal structure shown at right. OP, outer CuO_2 plane; IP, inner CuO_2 plane. (**C** to **K**) Cross-sectional layered structure in the Bi-family cuprates with $1 \le n \le 9$, where the c axis direction is along the vertical blue arrow. The yellow arrows indicate the positions of CuO_2 planes in the crystal (fig. S4). Scale bar, 5 Å. All the data were taken at T = 300 K.

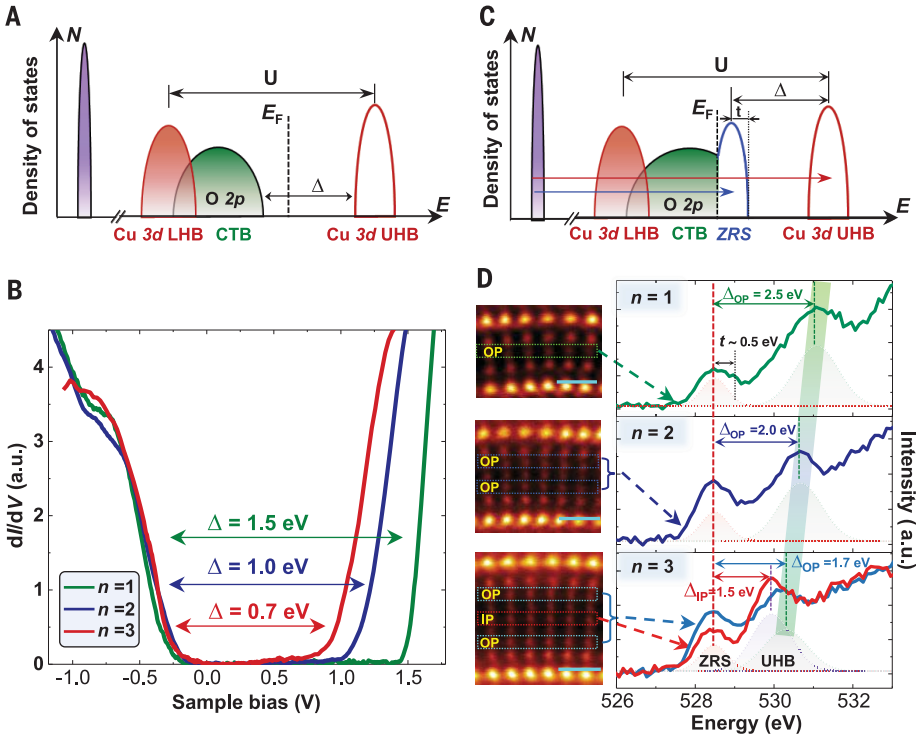

Fig. 2. Probing Δ with STM and STEM-EELS techniques. (**A**) Schematic band structure of the undoped cuprates. LHB, lower Hubbard band; CTB, charge transfer band; UHB, upper Hubbard band. (**B**) The Mott-insulator type d*I*/d*V* (differential conductance) spectra of undoped Bi-2201 (n = 1), Bi-2212 (n = 2), and Bi-2223 (n = 3) samples taken with STM. The Δ here characterizes the distance between the edges of CTB and UHB, as shown in (A). (**C**) Schematic band structure of hole-doped cuprates. ZRS, Zhang-Rice singlet. The red and blue arrows indicate the EELS excitation process from core levels to the unoccupied UHB and ZRS, respectively (the principle is shown in fig. S6). (**D**) STEM-EELS of the O *K* edge from n = 1 to 3. The Δ here characterizes the distance between the centers of ZRS and UHB, as shown in (C). The Gaussian functions were used to simulate the ZRS (red dotted lines) and the UHB (purple, IP; green, OP). (Left) The STEM images show the real-space areas where the EELS are taken. All the STEM-EELS data were taken at T = 300 K. a.u., arbitrary units.

and UHB is still a valid parameter that characterizes the charge-transfer energy (*27*), which varies little with doping (*28*, *29*). The state-of-the-art STEM-EELS is an ideal technique for measuring such peak-to-peak CTG, where the spectral peaks shown in Fig. 2D indicate the large probability of exciting core-level electrons to the unoccupied ZRS and UHB in Fig. 2C (*27*), in analogy to the x-ray absorption spectroscopy (XAS) at the O *K* edge (excitation energy of an O 1*s* core electron to an empty state). In particular, the ZRS peak centered around 528.5 eV (Fig. 2D, red dashed line) corresponds well with the measurements of the bulk-sensitive XAS technique (*27*). The ZRS peak is robust in cuprates against doping, temperature, and materials.

Similar to that of STM, the Δ obtained with EELS is mainly controlled by the unoccupied UHB, which displays a red-shift trend from n = 1 to 3, as revealed in Fig. 2D. We extracted the Δ size from a reliable fitting procedure as described in (*30*), which renders Δ = 2.5 eV for Bi-2201 and Δ = 2.0 eV for Bi-2212, respectively. Owing to the high atomic-plane resolution, we distinguished the CTG corresponding to the OP (Δ_{OP} = 1.7 eV) and IP (Δ_{IP} = 1.5 eV) in trilayer Bi-2223. The spectral weight ratio between the ZRS and UHB is smaller in the IP, which is suggestive of the lower hole concentration (*27*).

Correlating observables with the number of CuO_2 layers.

To investigate how the Δ size evolves with the number of CuO_2 layers per unit cell, we have further determined the STEM-EELS of the O *K* edge with $1 \le n \le 9$ (Fig. 3, A and B). The definition and description of different CuO_2 planes where we took the STEM-EELS measurements are shown in fig. S7. We repeated the measurements 10 times on different areas with the same n to improve statistical robustness (full dataset is provided in figs. S8 to S17) (*30*). For clarity, we only show the averaged spectra for the OP layer; those for the IP layers are shown in fig. S19. The overall trend is shown in Fig. 3, C and D, which clearly demonstrate that the n dependence of Δ is represented by an inverted bell-shaped curve with the minimum Δ = 1.8 eV at n = 3. There is an apparent anticorrelation between the n dependence of Δ and $T_{c,max}$. For all the phases in which $n \ge 3$, the Δ value of the IP is smaller than the Δ value of OP, but exhibits the same dependence on n (Fig. 3D).

In the scenario of single-band Hubbard model, we may define an effective superexchange energy $J_{eff} \sim 4t^2_{eff}/\Delta$, where t_{eff} is the effective hopping term that is proportional to t^2_{pd}/Δ, and t_{pd} is the hopping integral between neighboring O 2*p* and Cu 3*d* orbitals (*8*). Because the J_{eff} between local Cu moments has been proposed to be responsible for the spin singlet pairing (*31*), $J_{eff} \sim 1/\Delta^3$ thus correlates the CTG and the Cooper pairing strength. For n = 1 and 2, only the OP is present, and the increase of J_{OP} is consistent with that derived through STM (*9*) and inelastic photon scattering (*32*). For the whole range with $1 \le n \le 9$, Fig. 3E shows that the n dependence of J_{eff} for the OP layer exhibits a bell shape highly analogous to that of $T_{c,max}$. It reaches a peak at n = 3 and decreases for $4 \le n \le 9$. The close correlation between J_{eff} and $T_{c,max}$ indicates that the Δ, and thus the underlying strong correlation effects, determine $T_{c,max}$, at least in the Bi-family cuprates with $1 \le n \le 9$.

The combined STEM-EELS and STM results here touch on the central issue regarding the bell-shaped evolution of $T_{c,max}$ with n, which is universal in all cuprate families. From the theoretical point of view, a previous study (*4*)

has proposed that the enigmatic balance between Josephson tunneling and competing electronic orders is the underlying physical mechanism. Our results reveal that it is the CTG, which displays an inverted bell-shaped trend compared with the $T_{c,max}$ that plays a deterministic role in this empirical rule. This conclusion is supported by the consistency of Δ characterized by energy scales between band centers (EELS and XAS) and edges (STM). We summarize the CTG sizes taken with different experimental probes in Fig. 4. The difference between STM and EELS shows a rigid shift of ~1 eV, which is caused by the finite bandwidths and provides useful information about the

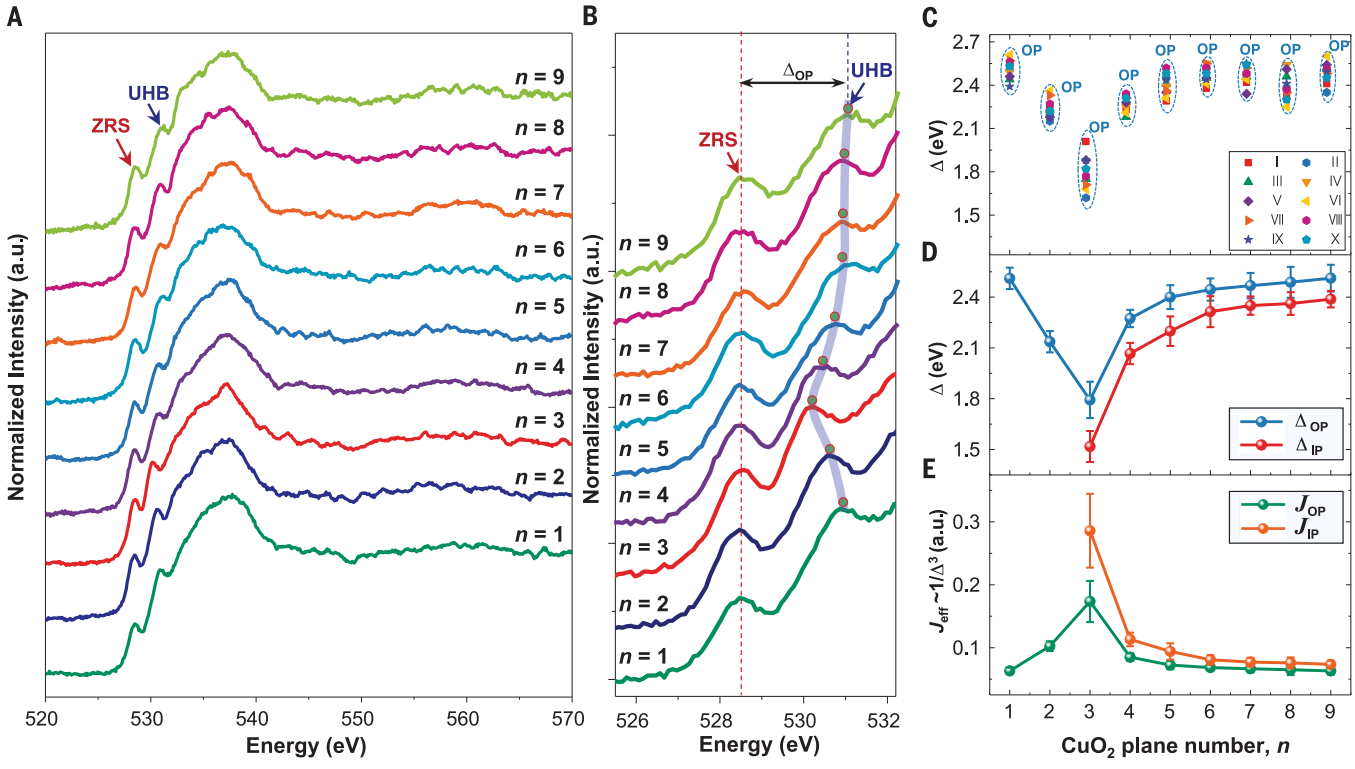

Fig. 3. The evolution of Δ with *n* in Bi-family cuprates. (**A**) STEM-EELS with a higher energy range of the O *K* edge with $1 \le n \le 9$. For each curve, we averaged the data measured on the OP layer of 10 different areas with the same *n* (full datasets are provided in figs. S8 to S17). (**B**) Zoomed-in STEM-EELS of (A). The Gaussian functions were used to determine the position of ZRS and UHB (fig. S18). (**C** and **D**) The statistical results of Δ for the OP and IP with $1 \le n \le 9$, which was determined with 10 measurements taken under the same experimental conditions. All the data were taken at T = 300 K. Each dot and error bar in (D) are the calculated average and standard deviation of the result in (C) for the same *n*. (**E**) The effective superexchange $J_{eff} \sim 1/\Delta^3$ as a function of *n*, assuming the same t_{eff} for the OP and IP of different *n* in a homologous series. a.u., arbitrary units.

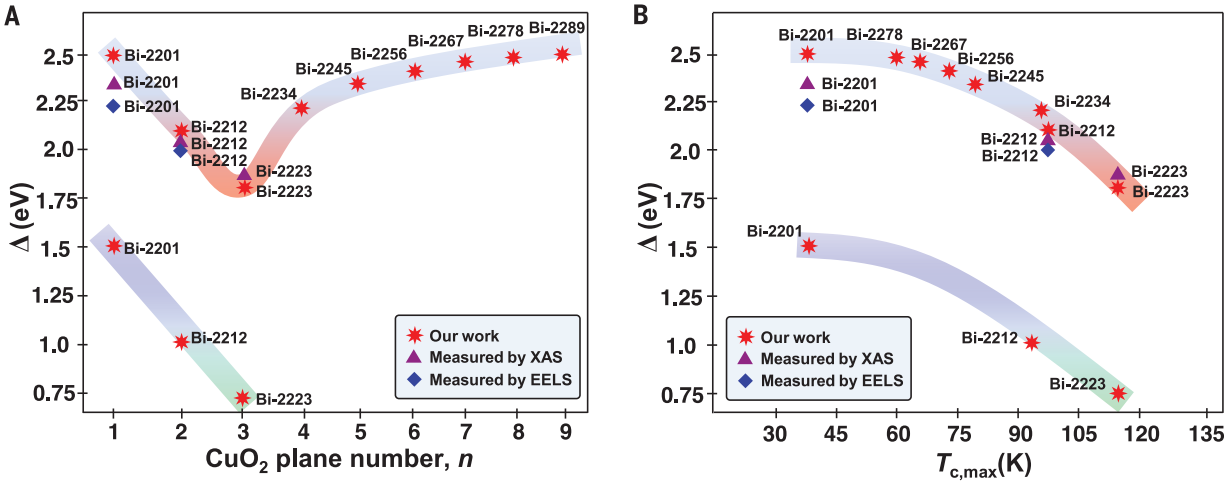

Fig. 4. The correlation between Δ, *n*, and $T_{c,max}$. (**A** and **B**) Summarized plots of (A) Δ versus *n* and (B) Δ versus $T_{c,max}$ for the Bi-family cuprates. Our STM and EELS (on the OP) data, as well as previous XAS data, are shown together. The STM results are generally ~1 eV smaller than the EELS and XAS values, owing to the finite bandwidth or hopping integral *t*. The wide gray-red and blue-green strips are guides to the eye. See table S1 for more details.

effective hopping integral in the Bi-family cuprates.

Discussion and outlook

Our study shows that the CuO_2 planes with different apical environments have very different Δ, which is seen not only in the evolution with n but also in that the IP always has a smaller Δ size than the OP of the same compound. The J_{eff} of IP is thus larger than that of OP, as shown in Fig. 3E, which is consistent with previous studies of the pairing strength (*21*, *33*). Therefore, the ultimate reason why Δ, and hence $T_{c,max}$, varies substantially for different n in a homologous series is most likely related to the orbitals out of the CuO_2 plane, indicating an interplay between the underlying electronic structure and orbital parameter symmetry in cuprates (*4*, *34*, *35*).

REFERENCE AND NOTES

1. B. Keimer, S. A. Kivelson, M. R. Norman, S. Uchida, J. Zaanen, *Nature* **518**, 179–186 (2015).
2. C. A. Reynolds, B. Serin, W. H. Wright, L. B. Nesbitt, *Phys. Rev.* **78**, 487 (1950).
3. E. Maxwell, *Phys. Rev.* **78**, 477 (1950).
4. S. Chakravarty, H.-Y. Kee, K. Völker, *Nature* **428**, 53–55 (2004).
5. C. W. Zou *et al*., *Nat. Phys.* **18**, 551–557 (2022).
6. T. Fujii, T. Watanabe, A. Matsuda, *Physica C Supercond* **357–360**, 173–176 (2001).
7. Z. Hao *et al*., *Phys. Rev. Lett.* **125**, 237005 (2020).
8. P. A. Lee, N. Nagaosa, X. G. Wen, *Rev. Mod. Phys.* **78**, 17–85 (2006).
9. W. Ruan *et al*., *Sci. Bull.* **61**, 1826–1832 (2016).
10. C. Weber, C. Yee, K. Haule, G. Kotliar, *Europhys. Lett.* **100**, 37001 (2012).
11. N. Kowalski, S. S. Dash, P. Sémon, D. Sénéchal, A.-M. Tremblay, *Proc. Natl. Acad. Sci. U.S.A.* **118**, e2106476118 (2021).
12. Z. H. Cui *et al*., *Phys. Rev. Res.* **2**, 043259 (2020).
13. D. A. Muller *et al*., *Science* **319**, 1073–1076 (2008).
14. H. Mukuda *et al*., *J. Phys. Soc. Jpn.* **81**, 011008 (2012).
15. C. W. Chu, L. Z. Deng, B. Lv, *Physica C* **514**, 290–313 (2015).
16. *Bismuth-Based High-Temperature Superconductors*, H. Maeda, Ed. (CRC Press, 1996).
17. H. Wang *et al*., *Appl. Phys. Lett.* **57**, 710–711 (1990).
18. H. Narita, T. Hatano, K. Nakamura, *J. Appl. Phys.* **72**, 5778–5785 (1992).
19. I. Bozovic, J. N. Eckstein, G. F. Virshup, *Physica C* **235**, 178–181 (1994).
20. C. Zou *et al*., *Phys. Rev. Lett.* **124**, 047003 (2020).
21. S. Kunisada *et al*., *Science* **369**, 833–838 (2020).
22. Y. Yu *et al*., *Nature* **575**, 156–163 (2019).
23. V. J. Emery, *Phys. Rev. Lett.* **58**, 2794–2797 (1987).
24. J. Zaanen, G. A. Sawatzky, J. W. Allen, *Phys. Rev. Lett.* **55**, 418–421 (1985).
25. F. C. Zhang, T. M. Rice, *Phys. Rev. B Condens. Matter* **37**, 3759–3761 (1988).
26. P. Cai *et al*., *Nat. Phys.* **12**, 1047–1051 (2016).
27. C. T. Chen *et al*., *Phys. Rev. Lett.* **66**, 104–107 (1991).
28. Y. Zhong *et al*., *Phys. Rev. Lett.* **125**, 077002 (2020).
29. C. Hu *et al*., *Nat. Commun.* **12**, 1356 (2021).
30. Materials and methods and additional data are available as supplementary materials.
31. P. W. Anderson, *Science* **235**, 1196–1198 (1987).
32. L. Wang *et al*., *Nat. Commun.* **13**, 3163 (2022).
33. H. Kotegawa *et al*., *Phys. Rev. B Condens. Matter* **64**, 064515 (2001).
34. E. Pavarini, I. Dasgupta, T. Saha-Dasgupta, O. Jepsen, O. K. Andersen, *Phys. Rev. Lett.* **87**, 047003 (2001).
35. T. Xiang, J. M. Wheatley, *Phys. Rev. Lett.* **77**, 4632–4635 (1996).
36. Z. C. Wang *et al*., Source Data for: Correlating the charge transfer gap to the maximum transition temperature in $Bi_2Sr_2Ca_{n-1}Cu_nO_{2n+4+\delta}$, version 1, Zenodo (2023); https://doi.org/10.5281/zenodo.7608360.

ACKNOWLEDGMENTS

We gratefully acknowledge Q. K. Xue for helpful discussions and assistance. **Funding:** This work was financially supported by the Chinese National Natural Science Foundation (Basic Science Center Project of NSFC, grant no. 52388201), the Basic and Applied Basic Research Major Programme of Guangdong Province, China (grant no. 2021B0301030003), and Jihua Laboratory (project no. X210141TL210). Y.W. is supported by the Innovation Program for Quantum Science and Technology (grant no. 2021ZD0302502) and the New Cornerstone Science Foundation through the New Cornerstone Investigator Program and the XPLORER PRIZE. X.Z. is supported by the Chinese National Natural Science Foundation of China (grant no. 11888101), the National Key Research and Development Program (grant no. 2021YFA1401800), and the Strategic Priority Research Program (B) of the Chinese Academy of Sciences (grant no. XDB25000000). This work used the resources of the National Center for Electron Microscopy in Beijing. **Author contributions:** J.Z. and Z.W. initiated the idea and designed the studies. Z.W. performed the electron microscopy experiments and data analysis with the help of J.Z. C.L. grew the crystals of Bi-2223. C.Z., X.L., H.Y., C.Y. and X.Z. processed the samples. C.Z. and Y.W. performed the STM experiment. All authors contributed to the scientific discussions. Y.X. offered some theoretical guidance on the DFT calculation. Z.W., C.Z., Y.W., and J.Z. wrote the paper with contributions from all authors. **Competing interests:** The authors declare that they have no competing interests. **Data and materials availability:** All data needed to evaluate the conclusions in the paper are deposited in a public database of Zenodo (*36*).

SUPPLEMENTARY MATERIALS

science.org/doi/10.1126/science.add3672
Materials and Methods
Figs. S1 to S20
Table S1
References (*37*–*47*)

Submitted 7 June 2022; accepted 6 June 2023
10.1126/science.add3672